

# An All-digital 65-nm Tsetlin Machine Image Classification Accelerator with 8.6 nJ per MNIST Frame at 60.3k Frames per Second

Svein Anders Tunheim<sup>✉</sup>, Senior Member, IEEE, Yujin Zheng<sup>✉</sup>, Lei Jiao<sup>✉</sup>, Senior Member, IEEE, Rishad Shafik<sup>✉</sup>, Senior Member, IEEE, Alex Yakovlev<sup>✉</sup>, Fellow, IEEE and Ole-Christoffer Granmo<sup>✉</sup>

arXiv:2501.19347v1 [cs.LG] 31 Jan 2025

**Abstract**—We present an all-digital programmable machine learning accelerator chip for image classification, underpinning on the Tsetlin machine (TM) principles. The TM is a machine learning algorithm founded on propositional logic, utilizing sub-pattern recognition expressions called clauses. The accelerator implements the coalesced TM version with convolution, and classifies booleanized images of  $28 \times 28$  pixels with 10 categories. A configuration with 128 clauses is used in a highly parallel architecture. Fast clause evaluation is obtained by keeping all clause weights and Tsetlin automata (TA) action signals in registers. The chip is implemented in a 65 nm low-leakage CMOS technology, and occupies an active area of  $2.7 \text{ mm}^2$ . At a clock frequency of 27.8 MHz, the accelerator achieves 60.3k classifications per second, and consumes 8.6 nJ per classification. The latency for classifying a single image is  $25.4 \mu\text{s}$  which includes system timing overhead. The accelerator achieves 97.42%, 84.54% and 82.55% test accuracies for the datasets MNIST, Fashion-MNIST and Kuzushiji-MNIST, respectively, matching the TM software models.

**Index Terms**—Tsetlin machine, Accelerator, Machine learning, Image classification.

## I. INTRODUCTION

**H**ARDWARE (HW) accelerators are commonly integrated in modern electronic systems to relieve the burden on system processors from extensive application-specific workloads. Performance and energy efficiency within a smaller form factor are key considerations for accelerator designs, particularly for Internet-of-Things (IoT), where the compute and memory resources of edge nodes typically are limited. In addition, such nodes are often battery-operated, and it is critical to minimize the overall energy footprints for longer battery operational lifetime.

Image classification is a key machine learning (ML) application, with usage scenarios across a wide range of IoT applications [1], such as industrial machine-vision, agricultural monitoring, unmanned aerial vehicles, room occupancy detection for building control systems, attention detection and gesture recognition.

Current methods of accelerating image classification in embedded systems, are predominantly based on convolutional neural networks (CNNs) [2], [3]. CNNs comprise many layers of multiply-and-accumulate (MAC) operations, each with their associated memory resources. As such, they require large number of micro-architectural operations for each classification

and have significant energy footprints [3]. The complexity and energy consumption can be reduced by compromising the data precision in CNNs [4]. Binary and ternary activations and weights have been applied in several integrated circuit (IC) solutions that have shown good test accuracy with very low power consumption [5]–[9].

Vision Transformer (ViT) [10] solutions obtain the highest score on image classification benchmarks, but they are computationally more intensive than CNNs [11]. ViT-based neural networks utilize a global receptive field that captures correlations between patches in an image [10], [11]. This is in contrast to CNNs, where convolutional layers extract features of an image in a hierarchical manner, with a limited local receptive field. Lightweight Transformer models have been developed, e.g., MobileViT [12], that have been applied for HW implementation [13].

Unlike the numerical models based on neural networks mentioned above, the Tsetlin machine [14] is an ML algorithm founded on propositional logic. During training, parallel conjunctive *clauses* are defined by independent learning automata. Each clause represents a logical sub-pattern and will output a logical 1 if it matches an input sample, and 0 otherwise. The TM features a single-layer structure with highly interpretable outputs [15]–[17], making it well-suited for application areas such as biomedical, cybernetics, IoT, and law, where interpretability is essential. Furthermore, because its primary operations are Boolean, TM solutions are both low-complexity and hardware-efficient. The generation of a TM’s output relies on summing and comparing class sums, with minimal or no need for energy-intensive multiplication operations, even during training. This makes TMs ideal for low-energy application-specific integrated circuit (ASIC) implementations [18]. Additionally, due to their small resource footprint, TMs facilitate hardware solutions that support on-device training and continuous learning [19], [20].

When compared against deep neural networks (DNNs) and other ML algorithms, the TM has demonstrated competitive performance. It has been tested on tabular data [14], natural language [15], [17], images [21]–[23] and regression [24]. Through the works in [25]–[27] the convergence of the TM’s basic operators has been verified.

The original TM version [14] is called the *vanilla TM*. For

image classification, improved test accuracy is achieved by the *convolutional TM (CTM)* [21]. The CTM has obtained a peak test accuracy of 99.4% on the MNIST dataset [28]. For the Fashion-MNIST (FMNIST) [29] and Kuzushiji-MNIST (KMNIST) [30] datasets, the peak test accuracies achieved are 91.5% and 96.31% respectively. Ensemble TM approaches have shown promising accuracies for more complex image datasets, such as CIFAR-10 and CIFAR-100, which are currently being investigated. In the case of CIFAR-10, the approach denoted *TM Composites* [31] has demonstrated a test accuracy of 82.8% [32].

In this paper, we present an all-digital inference accelerator ASIC based on the *coalesced TM* (CoTM) [22]. The CoTM utilizes a single clause pool, in contrast to the vanilla TM which uses one pool of clauses per class. As we operate the CoTM with convolution, we here denote it as a *convolutional CoTM (ConvCoTM)*. For configurations with few clauses, the ConvCoTM achieves better accuracy than the vanilla CTM, which makes the ConvCoTM especially attractive for HW solutions with constrained resources.

The main motivation behind the development of this ASIC was to demonstrate the HW friendliness and power efficiency of a ConvCoTM-based accelerator. The *main contributions* of this paper are:

- The accelerator is the first reported manufactured ASIC based on the CoTM. It is also the first TM ASIC where convolution is utilized.
- The ConvCoTM accelerator core operates with an energy per classification (EPC) of 8.6 nJ. To the best of the authors' knowledge, this is the lowest reported EPC for manufactured ASICs that operate on a similar test dataset and with comparable test accuracy.
- The accelerator has low latency, essential for real-time operation in low-power systems with strict requirements.
- The ConvCoTM solution is a fully digital, synchronous design compatible with standard digital workflows.

The remainder of the paper is organized as follows: Section II summarizes related work. Section III covers TM and CoTM background, including convolution operation. Section IV details the ASIC's architecture and building blocks. Measurement results are presented in Section V, followed by a discussion in Section VI before we conclude the paper.

## II. RELATED WORK

In this section, we describe state-of-the-art works on low-power inference accelerators for image classification, as well as some reported TM-based HW solutions.

For low-power neural networks, digital Binary Neural Networks (BNNs) are widely utilized. A BNN-based accelerator IC module is detailed in [33]. This module was later included in a complete system-on-chip (SoC) [6]. When operating on the CIFAR-10 [34] dataset, the SoC achieves 15.4 inferences/s and has a peak power envelope of 674  $\mu$ W. A 22 nm fully depleted silicon on insulator (FD-SOI) technology was used for the IC implementation.

In [7] a digital 10 nm FinFET CMOS solution is reported. Utilizing a BNN algorithm, it achieves a peak energy efficiency of 617 TOPS/W (Tera operations per second per watt).

It has a power consumption of 5.6 mW and obtains an accuracy of 86% when operating on the CIFAR-10 dataset.

An architecture for a binary-weight CNN is described in [8]. Images of size  $224 \times 224 \times 3$  are classified at a rate of 11 frames per second (FPS). The technology used is 65 nm CMOS and simulations show a power consumption of 895  $\mu$ W at 0.6 V.

The accelerator ASIC in [35] is manufactured in 65 nm CMOS. Its classification rates for Imagenet [36] are 35/0.7 FPS for the AlexNet and VGG-16 models respectively. The ASIC consumes 278 mW/236 mW with corresponding EPC values of 7.9 mW/0.4 mJ. The successor to [35] is the work described in [37]. Here, additional steps are taken to reduce energy consumption further. In particular, it reduces the movement of all data types during the various operational steps of the implemented CNN algorithm. A highly flexible on-chip network is utilized and sparse data are processed efficiently. When operating on  $224 \times 224 \times 3$  images from Imagenet, simulations show a power consumption of 1.44 mW at 1470.6 FPS. The technology used is 65 nm CMOS.

In-memory-computing (IMC) solutions can provide very high energy efficiency, as the bottleneck related to memory access is relieved. IMC has especially been utilized for analog/mixed-signal ML accelerator designs. An IMC mixed-signal 28 nm CMOS BNN processor is described in [5]. This accelerator achieves an EPC of 3.8  $\mu$ J when operating on CIFAR-10. The classification rate is 237 FPS with a power consumption of 0.9 mW.

In [9] a charge-domain IMC ternary neural network (TNN) classifier is described. The main advantage of the ternary approach is a reduction of the required operations per classification with  $3.9 \times$  compared to a BNN model. The accelerator classifies MNIST images at a rate of 549 FPS. It has very low power consumption, only 96  $\mu$ W, which corresponds to 0.18  $\mu$ J per classification. The test accuracy achieved is 97.1%.

Neuromorphic approaches, utilizing spiking neural networks (SNNs) have achieved very low energy consumption. In [38] a mixed-signal neuromorphic SNN IC is reported, which has been manufactured in a 65 nm CMOS technology. It achieves a test accuracy on MNIST of 95.35%, a power consumption of 0.517 mW and an EPC of 12.92 nJ. Simulation results of a 28 nm CMOS charge-domain computing SNN solution are reported in [39]. The accelerator achieves an EPC of 15.09 nJ, a latency of 0.46  $\mu$ s and a test accuracy on MNIST of 94.81%. In [40] simulation results of a clock-free, event-driven, mixed-signal 28 nm IMC SNN are described. On MNIST it achieves a test accuracy of 96.92% and 1.38 nJ EPC.

For the TM-based hardware solutions, the first reported IC is described in [18]. It utilizes the vanilla TM architecture and operates on a 3-class machine learning (ML) problem. The IC is implemented in a 65 nm CMOS technology and supports both training and inference. In [19], the first TM-based HW accelerator with convolution is reported. It is an FPGA solution which operates on a 2-class pattern recognition problem (two-dimensional noisy XOR [21]) in  $4 \times 4$  Boolean images, and employs a  $2 \times 2$  convolution window. Full on-device training is implemented.

The FPGA solution reported in [41] is based on the vanilla

TM and stores and processes only the *include* signals of the TA actions, utilizing the typical TM model's high sparsity. It therefore represents a highly compact implementation when it comes to HW resources. The design operates on the MNIST dataset, with sequential processing of each clause and each literal.

In [20] the first reported ConvCoTM-based HW solution is presented. It is an FPGA solution that classifies  $28 \times 28$  images with 10 categories, and includes complete on-device training. For the MNIST dataset a test accuracy of 97.6% is achieved, with a classification rate of 134k samples per second, and an EPC of  $13.3 \mu\text{J}$ .

Several articles describe the design and simulation of HW solutions for TM accelerators. In [42]–[44] low-latency asynchronous TM solutions for inference and training are presented. A mixed-signal IMC TM solution is described in [45] with an EPC for MNIST of  $13.9\text{nJ}$ . It is an inference solution with a Boolean-to-current architecture, and resistive RAM (ReRAM) transistor cells are employed to eliminate the need for energy-hungry analog-to-digital and digital-to-analog conversions. Another IMC TM concept based on Y-flash cells is reported in [46].

Based on the above literature review, developing a ConvCoTM ASIC solution is a critical step toward achieving higher energy efficiency, performance, and scalability for TM-based hardware accelerators. Existing FPGA implementations, while effective, are limited in energy efficiency. Comparatively, in-memory computing (IMC) and binary neural network (BNN)-based ASICs demonstrate significantly lower energy consumption and higher operational efficiency, underscoring the potential benefits of an ASIC approach. By leveraging a standard digital design flow and CMOS technology, an ASIC solution for ConvCoTM could deliver real-time, power-efficient classification. This would position ConvCoTM as a competitive alternative to CNNs and BNNs in resource-constrained environments.

### III. TM AND COTM BACKGROUND

The basic concepts of a vanilla TM [14] are described here, followed by a description of general CoTM inference [22]. Later, we explain how to apply convolution to the CoTM. As the emphasis in this paper is on *inference* solutions, we do not include details about CoTM/ConvCoTM training, except for a brief description of the Tsetlin automaton (TA), which is the core learning element in a TM. TM training is covered in detail in the original TM, CTM and CoTM references [14], [21], [22]. A compact description of ConvCoTM training can be found in [20].

#### A. General TM Concepts

The input feature vector to a TM consists of  $o$  propositional Boolean variables,  $x_u \in \{0, 1\}^o$ , where  $u \in \{0, \dots, o-1\}$ . A new input vector named the *literals*,  $L$ , is generated by appending the negated variables to the input, as shown in Eq. (1). Thus, there are in total  $2o$  literals.

$$\begin{aligned} L &= [l_0, l_1, \dots, l_{2o-1}] \\ &= [x_0, \dots, x_{o-1}, \neg x_0, \dots, \neg x_{o-1}] \end{aligned} \quad (1)$$

The Tsetlin Automaton (TA) of two-action type [47] constitutes the basic learning element in a TM. The TA will either *include* or *exclude* a literal in a conjunctive *clause*, depending on its state. One team of TAs is applied per clause, and the different TA actions are obtained during the training process which involves feedback mechanisms to each TA [14]. For an inference-only solution, as reported in this paper, we need only the *TA action signals* from the trained model, not the complete TAs.

In a TM the number of clauses,  $n$ , is a user specified integer. The output of a single clause,  $c_j$ , where  $j \in \{0, \dots, n-1\}$ , is given by

$$c_j = \bigwedge_{k \in I_j} l_k, \quad (2)$$

where  $l_k$  is the literal with index  $k$ .  $k$  belongs to  $I_j \subseteq \{0, \dots, 2o-1\}$ , where  $I_j$  is the set of literal indexes for clause  $j$  where the TA action is *include* [14].

#### B. CoTM

A vanilla TM employs one clause pool per class, and the clauses of each TM are grouped in two: positive and negative. In contrast, a CoTM [22] applies a single clause pool, common for all  $m$  outputs/classes. Different sets of weights,  $w_{i,j}$ , are applied to the clause outputs,  $\{c_0, \dots, c_{n-1}\}$ , to generate the class sums:

$$v_i = \sum_{j=0}^{n-1} w_{i,j} c_j, \quad (3)$$

where  $i \in \{0, \dots, m-1\}$  is the class index.

The clause weights in Eq. (3) obtain their values during training and can have both positive and negative polarity. It should be noted that *no multiplications* are needed to implement Eq. (3), only additions, as a clause can output only 0 or 1. The predicted class,  $\hat{y}$ , is determined by the *argmax* operator, as given by Eq. (4).

$$\hat{y} = \text{argmax}_i \{v_i\}, \quad i \in \{0, \dots, m-1\}. \quad (4)$$

#### C. CoTM and Convolution

One can improve the image classification test accuracy by applying convolution [21] to the CoTM. In addition, the number of features that need to be processed simultaneously, is lowered with convolution, which again reduces the model size and the complexity of a design. However, the benefits of convolution come at the expense of increased processing time, which is due to the need to sequentially process the different patches of the input sample.

For image classification, the input data samples to a ConvCoTM, are a set of images, each of dimensions  $X \times Y$ , with  $Z$  channels. The different patches of the image are generated by applying a sliding window of size  $W_X \times W_Y$ , with  $Z$  channels. The convolution window will be evaluated  $B = B_X \times B_Y$  times across the image, where  $B_X = 1 + (X - W_X)/d_x$ ,  $B_Y = 1 + (Y - W_Y)/d_y$ , and  $d_x$  and  $d_y$  are the stride values of the convolution window in

the  $X$  and  $Y$  directions respectively [21]. For each window position, the number of Boolean features is given by

$$N_F = W_X \times W_Y \times Z \times U + (Y - W_Y) + (X - W_X). \quad (5)$$

In Eq. (5),  $U$  is the number of bits used for thermometer encoding [48] of the value of a single pixel (one-hot encoding can also be used). Such encoding is required because a TM operates on Boolean variables, not on binary numbers. The term  $(Y - W_Y) + (X - W_X)$  in Eq. (5) represents the number of bits that encode the patch's position [22], [49] in the  $Y$  and  $X$  directions respectively. Also here we apply thermometer encoding. As shown in Eq. (1), the ConvCoTM also takes as input the negated versions of the features to form the *literals* per patch.

#### D. Datasets and Booleanization

The widely used MNIST [28] dataset consists of handwritten digits. FMNIST [29] is more challenging than MNIST and includes images from a Zalando catalog, such as t-shirts, sandals, and shoes. KMNIST [30] consists of cursive Japanese characters, and is also more demanding than MNIST. Each of these datasets includes images of  $28 \times 28$  pixels organized in 60k training samples and 10k test samples. There are 10 classes within each dataset. As the images are of single-channel (greyscale) type,  $Z = 1$ .

The pixel values range from 0 to 255. For MNIST, they are converted into Boolean variables (i.e., *booleanized*) with simple thresholding, where pixel values larger than 75 are replaced with 1, and 0 otherwise [21]. For FMNIST and KMNIST, the booleanization is performed with an adaptive Gaussian thresholding procedure [21]. Fig. 1 shows one example of an original image and the corresponding booleanized image from each of the three datasets. For the booleanized images the color white represents a logical 1.

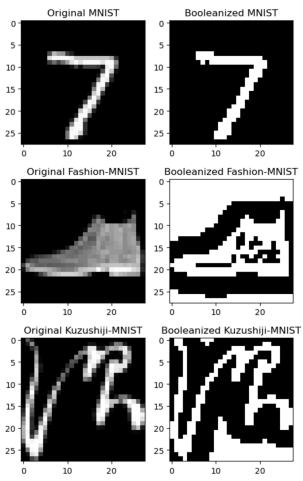


Fig. 1. Examples of MNIST, FMNIST and KMNIST image booleanization.

For the booleanization, we use one bit per pixel, i.e.,  $U = 1$  for all three datasets. The convolution window applied has dimensions  $W_X = W_Y = 10$ , and a step size of 1 is used in both directions. The number of feature bits per patch is

therefore 100 bits from the convolution window plus 36 bits for the appended patch position information, ref. Eq. (5). The number of literals for each patch is 272, i.e., two times the number of features.

#### E. TM and Convolution - Inference

During inference, each clause in a ConvCoTM is evaluated  $B$  times per image. After finishing the convolution, a clause will output 1 if it has recognized a pattern *at least once* in any of the  $B$  patches for a given image [21]. The clause output is given by the *sequential OR-function* in Eq. (6), where  $c_j$  is the  $j$ 'th clause of the ConvCoTM, and  $c_j^b$  is the  $b$ 'th output of this clause obtained during the window sliding (patch generation).

$$c_j = \bigvee_{b=0}^{B-1} c_j^b, \quad (6)$$

Class sum generation and class prediction are similar to the case without convolution, and follow Eq. (3) and Eq. (4).

## IV. DESIGN OVERVIEW

The block diagram of the ConvCoTM accelerator is shown in Fig. 2. The accelerator includes all circuitry required for performing inference, and only minimal interaction with the system processor is required. The three main modules are i) a data interface for transfer of model parameters and image samples, ii) a module for model storage and iii) an inference core that performs classification of an image.

The main configuration parameter of a TM solution is the number of clauses. Due to chip area restrictions, we decided to implement a configuration with 128 clauses. The following subsections describe the different sub-modules and the accelerator's operation in detail.

#### A. Interface to the System Processor

An external system processor is required for i) applying a few single-bit control signals to the accelerator, ii) feeding data to the accelerator and iii) reading interrupt signals and class predictions from the accelerator. All other operations are performed by the accelerator.

The data interface towards the external system processor, is an 8-bit parallel type inspired by the ARM AXI Stream interface [50]. It is used for transferring model data to the accelerator during *load model mode*, and for transferring images in *inference mode*. When a classification operation is finished, the accelerator outputs an interrupt. In addition, it outputs a separate 8-bit signal consisting of the predicted class (4 bits) together with the true label of the sample (4 bits).

#### B. ConvCoTM Model Registers

The *model* of a given CoTM configuration consists of: i) the TA action signals (*include/exclude* signals) *per clause* and ii) the signed weights *per clause per class*. The TA action signals are stored in registers, readily available for simultaneous clause evaluation. These signals require  $272 \times 128 = 34816$  D flip-flops (DFFs). Registers are also applied for the

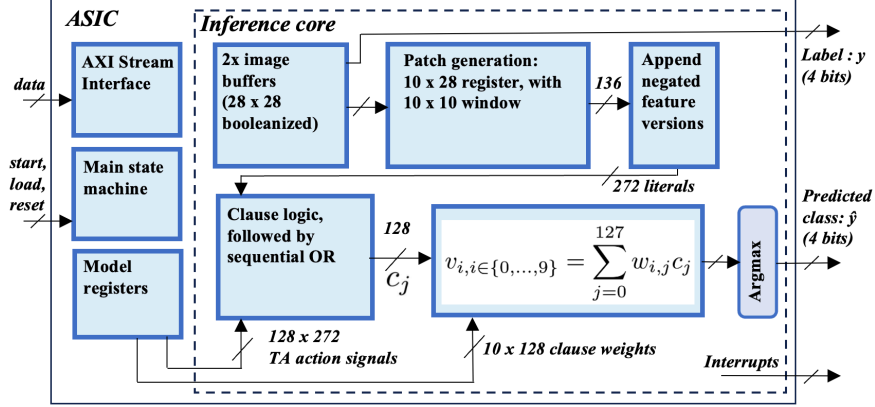


Fig. 2. ConvCoTM accelerator ASIC block diagram.

clause weights per class. For this ASIC, eight bits are allocated per weight, with two's complement representation. The number of DFFs for storing the weights is  $10 \times 128 \times 8 = 10240$ , and the complete model size used by the accelerator is 45056 bits, i.e., 5632 bytes.

### C. Image Data Buffer and Patch Generation

A data buffer is included with room for two complete  $28 \times 28$  booleanized images. While one image is being processed, another image can be transferred from the external system processor to the other image buffer, thereby improving throughput. We denote this as the *continuous* classification mode. A complete booleanized image requires  $28 \times 28 / 8 = 98$  bytes. In addition, one byte is allocated for the image label (0 to 9).

The patch generation module consists of a register with 10 rows, each with 28 DFFs. At the start of processing a new sample, the first 10 rows of an image are loaded into the register, and the convolution window starts at the leftmost position, which has coordinates (0,0).

During the convolution, the window is moved to the right with increments of one. As described in subsection III-C, the position of the window is thermometer encoded. There are 19 different  $x$ -coordinates for the window, requiring 18 bits. When the window has been evaluated at the rightmost  $x$ -position (0,18), the contents of all 10 rows are shifted upwards with one step, and the next image datarow is loaded into the lowermost row. Then the window starts again at the leftmost position, now with patch coordinates (1,0), and moves to the right in steps of one. This procedure is repeated until all 28 datarows of the image have been processed. Also for the  $x$ -coordinate, there are 19 different positions. During a complete convolution,  $19 \times 19 = 361$  patches are generated.

### D. Clause Pool

The ConvCoTM is configured with 128 clauses that operate in parallel. Each of the 128 clauses takes the literals,  $[l_0, l_1, \dots, l_{271}]$ , as input, as well as their corresponding *TA action* signals,  $[i_0, i_1, \dots, i_{271}]$ , from the model register. Fig. 3 shows a simplified circuit diagram of the clause logic. A literal will be included in the logical AND expression, that constitutes the *clause*, if its corresponding TA action signal is high. A special situation occurs when a clause is *empty*, i.e., when there are no *include* TA actions. In this case, additional logic will set the signal *Empty* high, forcing  $c_j^b$  low.

The DFF in Fig. 3 constitutes a single-bit register for clause  $j$ . During the convolution, its content,  $c_j$ , is ORed with the combinational clause value,  $c_j^b$ , of the current patch, thus implementing the *sequential OR function* in Eq. (6). Before starting a new convolution (patch generation), the DFF is reset.

The signal  $c_j$  is also fed back to the input of the OR-gates, as there is no need for the combinational logic to evaluate a clause for more patches if  $c_j$  already is high. This feedback mechanism, hereinafter denoted the *clause switching reduction feedback* (CSRF), reduces the digital switching in the combinational part of the clause logic. Simulations on MNIST image classification with CSRF enabled, showed an average of 50% reduction in the toggling rate of  $c_j^b$  for each clause. The accelerator ASIC has a dedicated pin that can enable or disable the CSRF.

In this accelerator ASIC we apply a single convolution window. If increased classification rate is wanted, one can use several convolution windows that operate in parallel. In this case, the combinational clause logic that generates the signal  $c_j^b$  in Fig. 3, would have to be replicated for each convolution window.

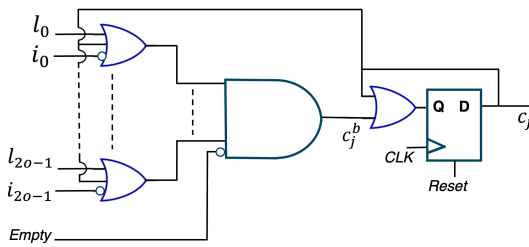


Fig. 3. Circuitry for a single clause. Literals are denoted with  $l$  and TA actions with  $i$ .

### E. Inference

The inference operation starts with loading an image into the data buffer, followed by a convolution process, as described in Subsection IV-C. When finished, each clause value,  $c_j$ , is weighted, for each class, according to Eq. (3).

All ten class sums are generated in parallel, by adders configured in a tree structure and utilizing a three-stage pipeline. Finally, an *argmax* module [18] selects the class with the highest class sum, as the *predicted class*,  $\hat{y}$ . Fig. 4 shows a simplified state diagram of the accelerator.

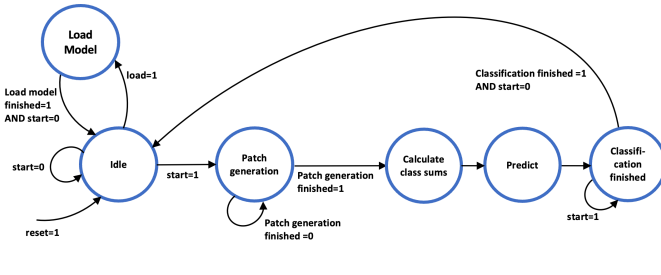


Fig. 4. Simplified accelerator state diagram.

The accelerator's latency, measured from when the system processor initiates the first byte transfer of the image, until a prediction result is available, is 471 clock cycles. This includes 99 clock cycles for transferring the 98 image bytes and the label byte, and 372 clock cycles for the patch generation and class prediction.

The accelerator can also operate in continuous mode, where a new sample is loaded into the image buffer while the current sample is being processed, see Subsection IV-C. This increases the throughput, as image samples can be processed every 372'th clock cycle. Any timing overhead in the system processor will add to the total latency.

### F. Clock Domains

The key to reducing the digital switching power of the accelerator ASIC lies at the top level of the ASIC architecture. Two separate clock domains are utilized, each with its own dedicated clock pin, assigned to i) the model part and ii) the inference core.

When a model has been transferred from the system processor to the ASIC, the TA action signals and the weights are available in registers which do not need further clocking. By stopping the clock to the model part when operating in inference mode, the digital switching power is reduced significantly, as the model part constitutes approximately 90% of the accelerator's DFFs. To further reduce power consumption, standard clock gating is applied for the inference module. This ensures, for instance, that the pipelined registers associated with the class sum generation are enabled and clocked only for 4 clock cycles per classification cycle. The clock-gating can be enabled/disabled by an external pin.

## V. IMPLEMENTATION AND MEASUREMENT RESULTS

The ConvCoTM accelerator was designed in VHDL and first implemented and verified on a Xilinx ZCU104 FPGA development board. The ASIC was then implemented in a 65 nm low-leakage CMOS technology from UMC, and packaged in a JLCC44 ceramic package. Fig. 5 shows a photograph and a layout plot of the ASIC. The accelerator's core area is 2.7 mm<sup>2</sup>.

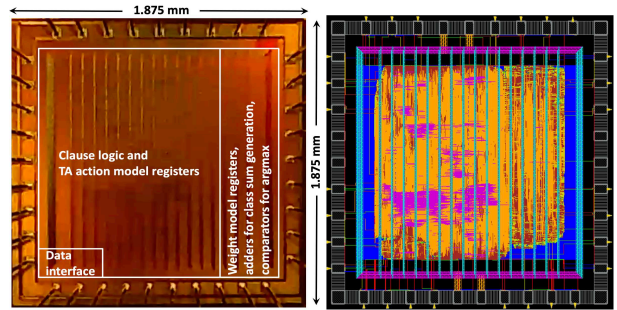


Fig. 5. Photo and layout plot of the ConvCoTM accelerator chip.

A test PCB was developed for the ASIC. This board was connected to a Digilent Zynq XC7Z020 development board equipped with a Xilinx Zynq XC7Z020 FPGA, as shown in Fig. 6. One of the FPGA's ARM9 cores was configured as system processor, and the FPGA board provided clocks, model data, image data samples and control signals to the ASIC accelerator. The processor also read back accelerator status/interrupt signals and the predicted/true class per sample. To interface with the FPGA board, the ASIC's input/output (IO) ports operated at 3.3 V supply voltage. The accelerator core operated from 0.82 V to 1.2 V.

For each of the datasets MNIST, FMNIST and KMNIST, the *Tsetlin Machine Unified* (TMU) SW-version [51] of

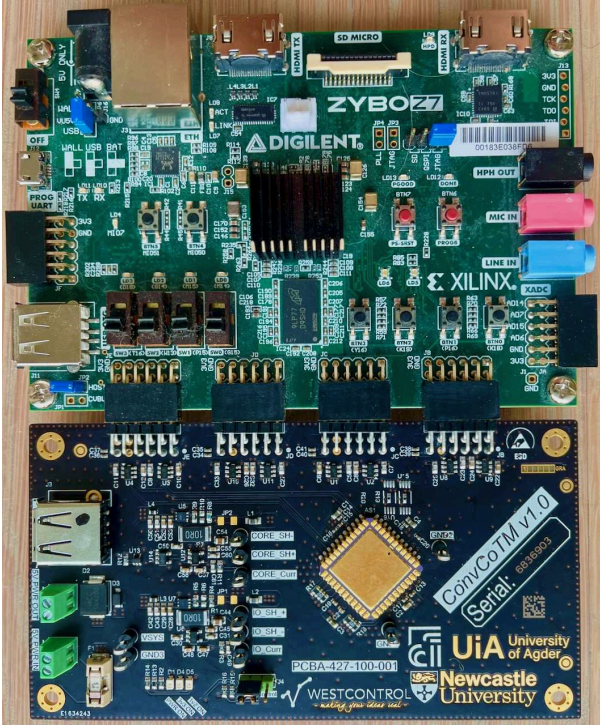


Fig. 6. Test setup with the ConvCoTM ASIC test board connected to the FPGA development board.

the ConvCoTM was trained to find suitable models. Maximum/minimum limits were set on the clause weights to fit with the allocated 8-bits per weight in the accelerator. For simplicity, the images from the test dataset were preprocessed (booleanized), as described in subsection III-D, and included in the FPGA processor's test program.

Model data and image samples were applied from the FPGA to the accelerator via the AXI Stream interface. We utilized DMA functionality on the FPGA to enable fast data transfer. The maximum classification rate achieved, including system processor timing overhead, was 60.3k images per second in continuous mode, with an accelerator clock frequency of 27.8MHz. The speed limiting factor was the electrical interface between the FPGA and the ASIC. The latency when classifying a single image was  $25.4 \mu\text{s}$ , including the transfer time of the image to the accelerator as well as timing overhead in the system processor.

The achieved test accuracies of the datasets MNIST, FMNIST and KMNIST were 97.42%, 84.54% and 82.55% respectively. These results are independent of the accelerator clock frequency and are exactly in accordance with the performance of the models obtained from the SW simulations.

In a real application, the ConvCoTM design would typically be included as a processor peripheral module in an SoC. Therefore, we considered the power consumption of the accelerator *core* as the most interesting performance power

parameter, and our measurements excluded energy consumed by the digital 3.3 V IOs of the ASIC. Table I summarizes the characteristics and performance of the accelerator.

TABLE I  
THE CONVCoTM ACCELERATOR ASIC'S MAIN CHARACTERISTICS AND PERFORMANCE

Parameter / Characteristics	Value / Description
Technology	65 nm low-leakage CMOS from UMC
Chip area (full die)	3.5 mm <sup>2</sup>
Chip area (core)	2.7 mm <sup>2</sup>
Gatecount (core)	201k cells including 52k DFFs
Power consumption (accelerator core only)	1.15 mW <sup>a,c</sup> 0.52 mW <sup>a,d</sup> 81 $\mu\text{W}$ <sup>b,c</sup> 21 $\mu\text{W}$ <sup>b,d</sup>
Classification rate (including system overhead)	60.3k images/s <sup>a</sup> 2.27k images/s <sup>b</sup>
Energy per classification (accelerator core only)	19.1 nJ <sup>a,c</sup> 8.6 nJ <sup>a,d</sup> 35.3 nJ <sup>b,c</sup> 9.6 nJ <sup>b,d</sup>
Latency (single image classification including data transfer)	25.4 $\mu\text{s}$ <sup>a</sup> 0.66 ms <sup>b</sup>
Test accuracy	97.42% (MNIST) 84.54% (FMNIST) 82.55% (KMNIST)

<sup>a</sup> 27.8 MHz clock frequency. <sup>b</sup> 1.0 MHz clock frequency. <sup>c</sup> The accelerator core supply voltage (vdd) is 1.20 V. <sup>d</sup> vdd=0.82 V.

For power consumption measurements, a Joulescope JS220 precision energy analyzer was used. The power consumption during inference was measured while the accelerator was set in a test mode with repeated classifications of the full 10k sample dataset. The power consumed by the accelerator core with 1.20 V supply voltage and a clock frequency of 27.8 MHz was 1.15 mW. This corresponds to an EPC of 19.1 nJ. With a supply voltage of 0.82 V, the power consumption was 0.52 mW and the corresponding EPC was 8.6 nJ. With 1.2 V core supply voltage and a clock frequency of 1 MHz, the achieved classification rate was 2.27k images/second at a power consumption of 81  $\mu\text{W}$ .

All power and energy measurement results of the ASIC are average values, and were performed with clock-gating and CSRF enabled (as shown in Fig. 3). When operating at 27.8 MHz, clock-gating reduced the power consumption by approximately 60%, while the CSRF alone provided less than 1% power reduction.

## VI. DISCUSSIONS

We consider the ConvCoTM solution with 128 clauses as a small configuration. In light of this, we are satisfied with the obtained test accuracy which is comparable with other low-complexity and low-power solutions. Table II shows the performance and properties of state-of-the-art low-power IC implementations for image classification. Inspired by the *TinyML* [52] benchmarks for embedded systems we specify the *classification rate*, the *peak power consumption* and the *EPC*. These are system parameters which are independent of the accelerator model and architecture [53]. However,

TABLE II  
COMPARISON OF THE CONVCoTM IC ACCELERATOR WITH PREVIOUS WORKS.

	This work	TCAS-II'23 Yejun [38]	JSSC'23 Yang [9]	TCAS-I'20 Mauro [6]	JSSC'21 Knag [7]	TCAS-I'20 Bankman [5]	JSSC'17 Chen [35]	JETCAS'19 Chen [37]
Technology	65 nm CMOS	65 nm CMOS	40 nm CMOS	22 nm FD-SOI	10 nm FinFET	28 nm CMOS	65 nm CMOS	65 nm CMOS
Active area	2.7 mm <sup>2</sup>	0.57 mm <sup>2</sup>	0.98 mm <sup>2</sup>	2.3 mm <sup>2</sup>	0.39 mm <sup>2</sup>	4.6 mm <sup>2</sup>	12.3 mm <sup>2</sup>	Not stated
Algorithm	ConvCoTM	SNN	Ternary CNN	BNN	BNN	BNN	CNN	Sparse DNN
Design type	Digital	Neuromorphic mixed-signal	IMC, mixed-signal	Digital (SoC)	Digital	IMC, mixed-signal	Digital	Digital
Image dataset	MNIST, FMNIST, KMNIST	MNIST	MNIST	CIFAR-10	CIFAR-10	CIFAR-10	Imagenet	Imagenet
Measured test accuracy	97.42%, 84.54%, 82.55%	95.35%	97.1%	99% of nominal accuracy	86%	86%	Not stated	79.6% <sup>i</sup> 79.7% <sup>j</sup>
Classifications per second	60.3k <sup>a</sup> 2.27k <sup>b</sup>	233k (1.2 V) 40k (0.7 V)	549	15.4	Not stated	237	35 <sup>g</sup> 0.7 <sup>h</sup>	278 <sup>j,i</sup> 1470 <sup>f,j</sup>
Latency <sup>e</sup>	25.4 $\mu$ s <sup>a</sup> 0.66 ms <sup>b</sup>	Not stated	Not stated	Not stated	Not stated	115.3 ms	Not stated	
Inference power	1.15 mW <sup>a,c</sup> 0.52 mW <sup>a,d</sup> 81 $\mu$ W <sup>b,c</sup> 21 $\mu$ W <sup>b,d</sup>	9.37 mW (1.2 V) 0.517 mW (0.7 V)	96 $\mu$ W	674 $\mu$ W	5.6 mW (13 MHz) 607 mW (622 MHz)	0.9 mW	278 mW <sup>g</sup> 236 mW <sup>h</sup>	Not stated
Energy per classification (EPC)	19.1 nJ <sup>a,c</sup> 8.6 nJ <sup>a,d</sup> 35.3 nJ <sup>b,c</sup> 9.6 nJ <sup>b,d</sup>	40.17 nJ (1.2 V) 12.92 nJ (0.7 V)	0.18 $\mu$ J	43.8 $\mu$ J	Not stated	3.8 $\mu$ J	7.9 mJ <sup>g</sup> 337 mJ <sup>h</sup>	1.5 mJ <sup>f,i</sup> 0.4 mJ <sup>f,j</sup>

<sup>a</sup> 27.8 MHz clock frequency. <sup>b</sup> 1.0 MHz clock frequency. <sup>c</sup> The accelerator core supply voltage (vdd) is 1.20 V. <sup>d</sup> vdd=0.82 V. <sup>e</sup> For processing of a single image sample, including data transfer. <sup>f</sup> Simulated results. <sup>g</sup> AlexNet. <sup>h</sup> VGG-16. <sup>i</sup> Sparse AlexNet. <sup>j</sup> Mobilenet.

when used for comparing solutions, one must be careful to specify the ML task performed. The ICs shown in Table II operate on images and datasets that range from low to high complexity. Accelerators that operate on CIFAR-10 and other more complex images, typically have lower classification rates and higher EPC compared to accelerators that operate on 28 × 28 images.

The mixed-signal IMC-based solution in [9] operates with a very low peak power consumption of 96  $\mu$ W and consumes 0.18  $\mu$ J per classification on MNIST with a test accuracy of 97.1%. Its classification rate is 549. In [38] a mixed-signal SNN IC accelerator achieves a very low EPC of 12.92 nJ with 0.7 V supply voltage. Operating at 1.2 V the EPC is 40.17 nJ. It utilizes a time-domain echo state network (ESN) [54] approach and thus requires non-standard interfacing with the surrounding system's resources. It obtains a test accuracy on MNIST of 95.35%.

To the authors' knowledge, the ConvCoTM accelerator core's EPC of 8.6 nJ at 0.82 V operating voltage is the lowest reported for a manufactured ASIC that classifies 28 × 28 greyscale images and which has comparable test accuracy. At 1.2 V operating voltage it obtains an EPC of 19.1 nJ, which is also very low. As the ConvCoTM ASIC is fully digital, the classification rate and thereby also the power consumption, can easily be scaled by adjusting the clock frequency. E.g., with a clock frequency of 1 MHz, the power consumption achieved is only 81  $\mu$ W. As the accelerator is all-digital, the test accuracy is independent of the clock frequency.

Several analog/mixed-signal IC accelerators obtain very low power consumption [5], [9], [38]. Such solutions are susceptible to variations in process parameters, supply voltage and operating temperature (PVT), which can affect the performance. All-digital solutions avoid such non-ideal effects [6]–[8]. In addition, they are easier to integrate in larger SoCs,

and can be scaled and re-targeted to other technologies. This applies for CNNs as well as for TMs.

In the ConvCoTM accelerator, the combinational clause logic draws only a small amount of energy compared to the clock tree of the inference-core DFFs. This is the main reason why the CSRF technique, see Subsection IV-D, did not provide a greater reduction in EPC. Other convolutional TM architectures, that operate at higher clock frequencies, process more literals in parallel, and utilize sparsity in TM models, can potentially benefit more from the CSRF technique.

The ConvCoTM accelerator's architecture described in this paper is highly suited for scaling. It can be modified to operate on larger images including 3-channel (RGB) images, e.g., based on the TM Composites architecture [31], [32]. From the very low energy consumption obtained for our ConvCoTM accelerator, we envisage that a TM Composites-based solution will perform well compared to previous works.

## VII. CONCLUSION

In this work, an ASIC implementation of a ConvCoTM accelerator for inference is presented. It operates on booleanized images of 28×28 pixels, and samples are classified into 10 categories. A pool of 128 clauses, i.e., pattern recognition logical expressions, is applied for the accelerator. The solution is fully programmable, and achieves a test accuracy of 97.42% on MNIST. With a clock frequency of 27.8 MHz, the accelerator's throughput is 60.3k images per second, and with an operating voltage of 0.82 V, the energy consumed by the accelerator core per classification is 8.6 nJ. To the authors' best knowledge this is lower than for previously reported fabricated ICs for the same classification task and for similar test accuracy.

The ASIC demonstrates the simplicity, hardware-friendliness and power-efficiency of TM solutions. We believe the TM represents an attractive ML solution for

low-power edge nodes in IoT systems. Furthermore, in a TM ASIC, full on-device training capabilities can be included, enabling adaptive edge solutions.

## ACKNOWLEDGMENTS

The authors would like to thank Adrian Wheeldon (Literal Labs, UK) and Jordan Morris (UK) for valuable general ASIC implementation discussions. Thank you also to Joel Trickey (STFC, UK) for support with IC design backend tools, and to Alberto Pagotto (imec.IC-Link, Belgium) for help during the ASIC tapeout phase. Finally, we would like to thank Geir Rune Angell (Westcontrol, Norway) for the design of the ASIC test board.

## REFERENCES

- [1] M. Maheepala, M. A. Joordens, and A. Z. Kouzani, “Low power processors and image sensors for vision-based IoT devices: A review,” *IEEE Sensors Journal*, vol. 21, no. 2, pp. 1172–1186, 2020.
- [2] Y. LeCun, “Deep learning hardware: Past, present, and future,” in *2019 IEEE International Solid-State Circuits Conference - (ISSCC)*, 2019, pp. 12–19.
- [3] V. Sze, Y.-H. Chen, T.-J. Yang, and J. S. Emer, “Efficient processing of deep neural networks: A tutorial and survey,” *Proceedings of the IEEE*, vol. 105, no. 12, pp. 2295–2329, 2017.
- [4] J. Dean, “The deep learning revolution and its implications for computer architecture and chip design,” in *IEEE ISSCC*, 2020, pp. 8–14.
- [5] D. Bankman, L. Yang, B. Moons, M. Verhelst, and B. Murmann, “An always-on 3.8  $\mu$ J/86% CIFAR-10 mixed-signal binary CNN processor with all memory on chip in 28-nm CMOS,” *IEEE JSSC*, vol. 54, pp. 158–172, 1 2019.
- [6] A. D. Mauro, F. Conti, P. D. Schiavone, D. Rossi, and L. Benini, “Always-on 674  $\mu$ W@4GOP/s error resilient binary neural networks with aggressive SRAM voltage scaling on a 22-nm IoT end-node,” *IEEE TCAS-I*, vol. 67, no. 11, pp. 3905–3918, 2020.
- [7] P. C. Knag, G. K. Chen, H. E. Sumbul, R. Kumar, S. K. Hsu, A. Agarwal, M. Kar, S. Kim, M. A. Anders, H. Kaul, and R. K. Krishnamurthy, “A 617-TOPS/W all-digital binary neural network accelerator in 10-nm FinFET CMOS,” *IEEE JSSC*, vol. 56, no. 4, pp. 1082–1092, 2021.
- [8] R. Andri, L. Cavigelli, D. Rossi, and L. Benini, “YodaNN: An architecture for ultralow power binary-weight CNN acceleration,” *IEEE TCAD*, vol. 37, pp. 48–60, 1 2018.
- [9] X. Yang, K. Zhu, X. Tang, M. Wang, M. Zhan, N. Lu, J. P. Kulkarni, D. Z. Pan, Y. Liu, and N. Sun, “An in-memory-computing charge-domain ternary CNN classifier,” *IEEE JSSC*, vol. 58, no. 5, pp. 1450–1461, 2023.
- [10] A. Dosovitskiy, L. Beyer, A. Kolesnikov, D. Weissenborn, X. Zhai, T. Unterthiner, M. Dehghani, M. Minderer, G. Heigold, S. Gelly, J. Uszkoreit, and N. Houlsby, “An image is worth 16x16 words: Transformers for image recognition at scale,” 2021. [Online]. Available: <https://arxiv.org/abs/2010.11929>
- [11] Y. Wang et. al, “An energy-efficient transformer processor exploiting dynamic weak relevances in global attention,” *IEEE JSSC*, vol. 58, no. 1, pp. 227–242, 2023.
- [12] S. Mehta and M. Rastegari, “MobileViT: Light-weight, general-purpose, and mobile-friendly vision transformer,” 2022. [Online]. Available: <https://arxiv.org/abs/2110.02178>
- [13] S.-F. Hsiao et. al, “Hardware accelerator for MobileViT vision transformer with reconfigurable computation,” in *2024 IEEE ISCAS*, pp. 1–4.
- [14] O.-C. Granmo, “The Tsetlin machine – A game theoretic bandit driven approach to optimal pattern recognition with propositional logic,” *arXiv e-prints*, 2018. [Online]. Available: <https://arxiv.org/abs/1804.01508>
- [15] B. Bhattacharai, O.-C. Granmo, and L. Jiao, “Word-level human interpretable scoring mechanism for novel text detection using Tsetlin Machines,” *Appl Intell*, 2022.
- [16] R. K. Yadav, L. Jiao, O.-C. Granmo, and M. Goodwin, “Robust interpretable text classification against spurious correlations using AND-rules with negation,” in *IJCAI*, 7 2022, pp. 4439–4446.
- [17] ———, “Human-level interpretable learning for aspect-based sentiment analysis,” *AAAI*, vol. 35, no. 16, pp. 14 203–14 212, May 2021.
- [18] A. Wheeldon, R. Shafik, T. Rahman, J. Lei, A. Yakovlev, and O.-C. Granmo, “Learning automata based energy-efficient AI hardware design for IoT applications,” *Philosophical Transactions of the Royal Society A: Mathematical, Physical and Engineering Sciences*, vol. 378, no. 2182, 2020.
- [19] S. A. Tunheim, L. Jiao, R. Shafik, A. Yakovlev, and O.-C. Granmo, “Convolutional Tsetlin machine-based training and inference accelerator for 2-D pattern classification,” *Microprocessors and Microsystems*, vol. 103, p. 104949, 2023.
- [20] ———, “Tsetlin machine-based image classification FPGA accelerator with on-device training,” *IEEE Transactions on Circuits and Systems I: Regular Papers*, vol. 72, no. 2, pp. 830–843, 2025.
- [21] O.-C. Granmo, S. Glimsdal, L. Jiao, M. Goodwin, C. W. Omlin, and G. T. Berge, “The convolutional Tsetlin machine,” *arXiv e-prints*, 2019. [Online]. Available: <https://arxiv.org/abs/1905.09688>
- [22] S. Glimsdal and O.-C. Granmo, “Coalesced multi-output Tsetlin machines with clause sharing,” *arXiv e-prints*, 2021. [Online]. Available: <https://arxiv.org/abs/2108.07594>
- [23] J. Sharma, R. Yadav, O.-C. Granmo, and L. Jiao, “Drop clause: Enhancing performance, robustness and pattern recognition capabilities of the Tsetlin machine,” *AAAI*, vol. 37, no. 11, pp. 13 547–13 555, 2023.
- [24] K. D. Abeyrathna, B. Bhattacharai, M. Goodwin, S. R. Gorji, O.-C. Granmo, L. Jiao, R. Saha, and R. K. Yadav, “Massively parallel and asynchronous Tsetlin machine architecture supporting almost constant-time scaling,” in *ICML*, vol. 139. Virtual: PMLR, 18–24 Jul 2021, pp. 10–20.
- [25] X. Zhang, L. Jiao, O.-C. Granmo, and M. Goodwin, “On the convergence of Tsetlin machines for the IDENTITY- and NOT operators,” *IEEE TPAMI*, June 2021.
- [26] L. Jiao, X. Zhang, O.-C. Granmo, and K. D. Abeyrathna, “On the convergence of Tsetlin machines for the XOR operator,” *IEEE TPAMI*, Aug. 2022.
- [27] L. Jiao, X. Zhang, and O.-C. Granmo, “On the convergence of Tsetlin machines for the AND and the OR operators,” *arXiv preprint*, 2021.
- [28] Y. LeCun and C. Cortes, “MNIST handwritten digit database,” 2010. [Online]. Available: <http://yann.lecun.com/exdb/mnist/>
- [29] Fashion-MNIST Repo., <https://www.openml.org/search?type=data&status=active&id=40996&sort=runs>, 2017.
- [30] Kuzushiji-MNIST Repo., <https://github.com/rois-codh/kmnist?tab=readme-ov-file>, 2019.
- [31] O.-C. Granmo, “TMComposites: Plug-and-play collaboration between specialized Tsetlin machines,” 2023. [Online]. Available: <https://arxiv.org/pdf/2309.04801.pdf>
- [32] Y. Grønningseter, H. S. Smørvik, and O.-C. Granmo, “An optimized toolbox for advanced image processing with Tsetlin machine composites,” *arXiv e-prints*, 2024.
- [33] F. Conti, P. Schiavone, and L. Benini, “XNOR neural engine: A hardware accelerator IP for 21.6 fJ/op binary neural network inference,” *IEEE TCAD*, vol. 37, pp. 2940–2951, 11 2018.
- [34] A. Krizhevsky, “Learning multiple layers of features from tiny images,” <https://www.cs.toronto.edu/~kriz/cifar.html>, 2009.
- [35] Y.-H. Chen, T. Krishna, J. S. Emer, and V. Sze, “Eyeriss: An energy-efficient reconfigurable accelerator for deep convolutional neural networks,” *IEEE JSSC*, vol. 52, no. 1, pp. 127–138, 2017.
- [36] J. Deng, W. Dong, R. Socher, L.-J. Li, K. Li, and L. Fei-Fei, “Imagenet: A large-scale hierarchical image database,” in *2009 IEEE conference on computer vision and pattern recognition*. Ieee, 2009, pp. 248–255.
- [37] Y.-H. Chen, T.-J. Yang, J. Emer, and V. Sze, “Eyeriss v2: A flexible accelerator for emerging deep neural networks on mobile devices,” *IEEE JETCAS*, vol. 9, pp. 292–308, 06 2019.
- [38] Y. Ko, S. Kim, K. Shin, Y. Park, S. Kim, and D. Jeon, “A 65 nm 12.92-nJ/inference mixed-signal neuromorphic processor for image classification,” *IEEE Transactions on Circuits and Systems II: Express Briefs*, vol. 70, no. 8, pp. 2804–2808, 2023.
- [39] Y. Zhang, Z. Xuan, and Y. Kang, “A 28nm 15.09nJ/inference neuromorphic processor with SRAM-based charge domain in-memory-computing,” in *2023 IEEE 15th International Conference on ASIC (ASICON)*, 2023, pp. 1–4.
- [40] W. Fang, Z. Xuan, S. Chen, and Y. Kang, “An 1.38nJ/inference clock-free mixed-signal neuromorphic architecture using ReL-PSP function and computing-in-memory,” in *2023 IEEE Biomedical Circuits and Systems Conference (BioCAS)*, 2023, pp. 1–5.
- [41] P. K. Sahu, S. Boppu, R. Shafik, S. A. Tunheim, O.-C. Granmo, and L. R. Cenkeramaddi, “Enhancing inference performance through include only literal incorporation in Tsetlin machine,” in *2023 International Symposium on the Tsetlin Machine (ISTM)*, 2023, pp. 1–8.

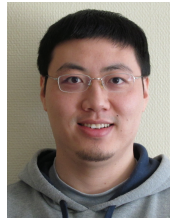
- [42] A. Wheeldon, A. Yakovlev, R. Shafik, and J. Morris, “Low-latency asynchronous logic design for inference at the edge,” in *2021 Design, Automation & Test in Europe Conference & Exhibition (DATE)*, 2021, pp. 370–373.
- [43] A. Wheeldon, A. Yakovlev, and R. Shafik, “Self-timed reinforcement learning using Tsetlin machine,” in *2021 27th IEEE International Symposium on Asynchronous Circuits and Systems (ASYNC)*, 2021, pp. 40–47.
- [44] T. Lan, O. Ghazal, S. Ojukwu, K. Krishnamurthy, R. Shafik, and A. Yakovlev, “An asynchronous winner-takes-all arbitration architecture for Tsetlin machine acceleration,” in *2024 22nd IEEE Interregional NEWCAS Conference (NEWCAS)*, 2024, pp. 16–20.
- [45] O. Ghazal, S. Singh, T. Rahman, S. Yu, Y. Zheng, D. Balsamo, S. Patkar, F. Merchant, F. Xia, A. Yakovlev, and R. Shafik, “IMBUE: In-memory boolean-to-current inference architecture for Tsetlin machines,” 2023.
- [46] O. Ghazal, T. Lan, S. Ojukwu, K. Krishnamurthy, A. Yakovlev, and R. Shafik, “In-memory learning automata architecture using Y-flash cell,” 2024. [Online]. Available: <https://arxiv.org/abs/2408.09456>
- [47] M. L. Tsetlin, “On behaviour of finite automata in random medium.” *Avtomat. i Telemekh.*, 22(10), pp. 1345–1354, 1961.
- [48] J. Buckman, A. Roy, C. Raffel, and I. Goodfellow, “Thermometer encoding: One hot way to resist adversarial examples,” in *ICLR*, 2018.
- [49] S. A. Tunheim, L. Jiao, and O.-C. Granmo, “Model export for the convolutional coalesced Tsetlin machine,” in *2023 International Symposium on the Tsetlin Machine (ISTM)*, 2023, pp. 1–4. [Online]. Available: <https://doi.org/10.1109/ISTM58889.2023.10455048>
- [50] AMBA AXI4 interface protocol , <https://www.xilinx.com/products/intellectual-property/axi.html>.
- [51] Tsetlin machine unified (TMU) CoTM github repository, [https://github.com/cair/tmu/blob/main/tmu/models/classification/coalesced\\_classifier.py](https://github.com/cair/tmu/blob/main/tmu/models/classification/coalesced_classifier.py), 2023.
- [52] C. B. et al., “MLPerf tiny benchmark,” 2021.
- [53] V. Sze, Y.-H. Chen, T.-J. Yang, and J. S. Emer, “How to evaluate deep neural network processors: TOPS/W (alone) considered harmful,” *IEEE Solid-State Circuits Magazine*, vol. 12, no. 3, pp. 28–41, 2020.
- [54] M. Lukoševičius and H. Jaeger, “Reservoir computing approaches to recurrent neural network training,” *Computer Science Review*, vol. 3, no. 3, pp. 127–149, 2009. [Online]. Available: <https://www.sciencedirect.com/science/article/pii/S1574013709000173>



**Stein Anders Tunheim** is a PhD research fellow at the University of Agder at Centre for Artificial Intelligence Research (CAIR). He completed his MSc degree in Electrical Engineering at The Norwegian University of Science and Technology (NTNU) in 1991. From 1992 to 1996 he worked as research scientist at SI (Senter for Industriforskning) and SINTEF within the field of mixed-signal integrated circuits (ICs). He was co-founder and Chief Technology Officer at Chipcon, a global supplier of low-power radio frequency ICs and radio protocols. From 2006 to 2008 he worked at Texas Instruments Norway as Technical Director for the Low Power Wireless product line. Currently, at CAIR, he is working on low-power hardware implementations of machine learning systems based on the Tsetlin Machine. He is a Senior Member of IEEE.



**Yujin Zheng** is a PhD candidate in the Microsystems Research Group at Newcastle University. She received her Master’s degree in Microelectronics at Newcastle University and a Bachelor’s in Applied Electronics from the University of Electronic Science and Technology of China (UESTC). Yujin was a senior board-level hardware engineer in China. She is currently working on ASIC implementation for hardware security.



**Lei Jiao** received the B.E. degree in telecommunications engineering from Hunan University, Changsha, China, in 2005, the M.E. degree in communication and information system from Shandong University, Jinan, China, in 2008, and the Ph.D. degree in information and communication technology from the University of Agder (UiA), Norway, in 2012. He is currently working as a Professor with the Department of Information and Communication Technology, UiA. His research interests include reinforcement learning, Tsetlin machine, resource allocation and performance evaluation for communication and energy systems.



**Rishad Shafik** is a Professor in Electronic Systems within the School of Engineering, Newcastle University, UK. Professor Shafik received his PhD, and MSc (with distinction) degrees from Southampton in 2010, and 2005; and BSc (with distinction) from the IUT, Bangladesh in 2001. He is one of the editors of the Springer USA book “Energy-efficient Fault-tolerant Systems”. He is also author/co-author of 200+ IEEE/ACM peer-reviewed articles, with 4 best paper nominations and 3 best paper/poster awards. He recently chaired multiple international conferences/symposiums, UKCAS2020, ISCAS2025, ISTM2022; guest edited a special theme issue in Royal Society Philosophical Transactions A; he is currently chairing 2nd IEEE SAS, 2025. His research interests include hardware/software co-design for energy-efficiency and autonomy.



**Alex Yakovlev** received the Ph.D. degree from the St. Petersburg Electrical Engineering Institute, St. Petersburg, USSR, in 1982, and D.Sc. from Newcastle University, UK, in 2006. He is currently a Professor of Computer Systems Design, who founded and leads the Microsystems Research Group, and co-founded the Asynchronous Systems Laboratory, Newcastle University. He was awarded an EPSRC Dream Fellowship from 2011 to 2013. He has published more than 500 articles in various journals and conferences, in the area of concurrent and asynchronous systems, with several best paper awards and nominations. He has chaired organizational committees of major international conferences. He has been principal investigator on more than 30 research grants and supervised over 70 Ph.D. students. He is a fellow of the Royal Academy of Engineering, UK.



**Ole-Christoffer Granmo** is the Founding Director of the Centre for Artificial Intelligence Research (CAIR), University of Agder, Norway. He obtained his master’s degree in 1999 and the PhD degree in 2004, both from the University of Oslo, Norway. In 2018 he created the Tsetlin machine, for which he was awarded the AI researcher of the decade by the Norwegian Artificial Intelligence Consortium (NORA) in 2022. Dr. Granmo has authored more than 160 refereed papers with eight paper awards within machine learning, encompassing learning automata, bandit algorithms, Tsetlin machines, Bayesian reasoning, reinforcement learning, and computational linguistics. He has further coordinated 7+ research projects and graduated 55+ master- and nine PhD students. Dr. Granmo is also a co-founder of NORA. Apart from his academic endeavours, he co-founded the companies Anzyz Technologies AS and Tsense Intelligent Healthcare AS.